PCCP

Accepted Manuscript

This is an *Accepted Manuscript*, which has been through the Royal Society of Chemistry peer review process and has been accepted for publication.

Accepted Manuscripts are published online shortly after acceptance, before technical editing, formatting and proof reading. Using this free service, authors can make their results available to the community, in citable form, before we publish the edited article. We will replace this *Accepted Manuscript* with the edited and formatted *Advance Article* as soon as it is available.

You can find more information about *Accepted Manuscripts* in the **Information for Authors**.

Please note that technical editing may introduce minor changes to the text and/or graphics, which may alter content. The journal's standard **Terms & Conditions** and the **Ethical guidelines** still apply. In no event shall the Royal Society of Chemistry be held responsible for any errors or omissions in this *Accepted Manuscript* or any consequences arising from the use of any information it contains.

www.rsc.org/pccp

Evaluating bulk Nb$_2$O$_2$F$_3$ for Li-battery electrode application

Rafael B. Araujo[1] and Rajeev Ahuja[1, 2]

[1]*Condensed Matter Theory Group, Department of Physics and Astronomy,*
Box 516, Uppsala University, S-75120 Uppsala, Sweden.
[2]*Applied Materials Physics, Department of Materials and Engineering,*
Royal Institute of Technology (KTH), S-100 44 Stockholm, Sweden

This investigation has the primary objective of to elucidate lithium intercalation process in the crystal structure of the new niobium oxyfluoride compound Nb$_2$O$_2$F$_3$. The framework of the density functional theory was applied in the generalized gradient approximation together with the hybrid functional method. It is revealed that lithium atoms intercalate in this material in a maximum concentration of one Li atom per formula unit forming LiNb$_2$O$_2$F$_3$. Moreover, octahedral positions in between the layers of Nb-O-F appear as the Li preferred occupancy resulting in a structural volume expansion of only 5%. The electronic structure evolution with the insertion of lithium displays a transformation from semi-conductor to metal when half of lithium atoms are added. This transformation occurs due to a symmetry break induced by the transition from +8 to +7 oxidation state of half of Nb$_2$ dimers. Then, after full lithiation the symmetry is recovered and the material becomes a semiconductor again with band gap amounting to 1 eV. The evaluated average deintercalation potential reaches 1.29 V vs. Li/Li$^+$ with activation energy for lithium ions migration of 0.79 eV. The computed low potential of the redox reaction Nb$_2^{+8}$ to Nb$_2^{+7}$ include niobium oxyfluoride to the map of possible material for anode application of Li-ion batteries.

I. INTRODUCTION

The research field of rechargeable lithium batteries has presented a systematic growth of interest by the scientific community in the recent years. This is a result of the heavy applicability of these devices in our daily life. One important topic into this field emerges from the search for materials with low discharge voltage vs. Li/Li$^+$. In fact, there exist two main possible applications where these materials with lower potential suits perfectly. The first case is to substitute the currently used LiC$_6$ anode material by one with slightly greater potential (1 V- 1.5 V vs. Li/Li$^+$). This substitution allows the application of cathode materials with higher voltage vs. lithium but still in the range of potential where the electrolyte remains stable [1–7]. The other possibility emerges as cathode application in powering back up of memory devices [3, 8–12].

On the basis of the low redox couple, low cost and non-toxicity, titanium and niobium based oxides have continuously been considered as interesting candidates for lower potential electrode materials. Many investigations have explored Ti based systems such as TiO$_2$ [13] and Li$_4$Ti$_5$O$_{12}$ [14, 15] or Nb based materials such as Li$_{1.714}$Nb$_2$O$_{10}$ [3] and LiNbO$_3$ [16]. These niobium based materials, for instance, deliver a potentials of 1.65 V and 1.67 V vs. Li/Li$^+$, respectively. The other possibility is also the mixture of both transition metals like Ti$_2$Nb$_{10}$O$_{29}$ [17] and LiTiNbO$_5$ [18] as stable anode for the recharge lithium battery.

This work comes with the objective of to investigate lithium intercalation process in niobium oxyfluoride, Nb$_2$O$_2$F$_3$, as possible candidate to the next generation of anode for Li-ion batteries. This compound was recently synthesized by Tran *et al.* [19] presenting low Nb oxidation state and an opened crystal framework susceptible to

intercalate lithium ions reversibly. Moreover, addition of Li atoms in the crystal structure of Nb$_2$O$_2$F$_3$ is followed by a reduction process of Nb ions to even lower oxidation states what is expected to deliver a quite small voltage vs. Li/Li$^+$. This small delivered potential should, then, indicate this material as a promising candidate for anode application of Li-ion batteries.

II. COMPUTATIONAL DETAILS

In order to derive the electronic and structural properties of the lithiated and delithiated niobium oxyfluoride phases the framework of the density functional theory in the projector augmented wave (PAW) method was applied as implemented in Vienna Ab initio Simulation Package (VASP) [20, 21]. All calculations were undertaken using spin polarized formalism and for the exchange correlation functional the Perdew, Burke, and Ernzerhof (PBE) [22] generalized gradient approximation was used. The screened hybrid functional of Heyd-Scuseria-Ernzerhof (HSE06) [23, 24] was also employed with the main objective of partially overcame the self-interaction error coming from PBE. The plane wave cutoff showed to be converged at 600 eV. Sampling of the Brillouin zone was considered in different k-meshs depending of the size of the supercell and the required property. In all cases, fractional coordinates as well as cell shape were relaxed until forces in each atom reach 0.01 Å^{-1}.

For the intercalation process of Li atoms in the Nb$_2$O$_2$F$_3$ crystal structure two schemes were followed. First a supercell of 2x2x1 was built up containing 56 atoms. Then, Li atoms were placed in non equivalent positions for each concentration x (x=0.25, 0.5, 0.75, 1, 1.25, 1.5 and 2) resulting in Li$_x$Nb$_2$O$_2$F$_3$ **(each**

structure containing 56, 58, 60, 64, 66, 70 and 74 atoms). In sequence, energy minimization process were carried out to ensure that these configurations have reached them ground state. Five distinct Li configuration were investigated in each concentration to ensure that a representative model was found. At this point of the investigation the generalized gradient approach was employed to treat the exchange and correlation term in a k-point Γ centered grid of 1x1x2.

In sequence, the structures presenting lowest total energy for each concentration were submitted to an *ab initio* molecular dynamics (AIMD) simulation in the canonical ensemble (fixed particle number, volume and temperature, NVT) at 600 K. The host atoms were kept fixed with only Li atoms migrating. The 600 K temperature helps to accelerate the dynamics and, as a whole, a 4 ps simulation were carried out to obtain the most probable adsorption sites for lithium ions in each concentration. The MD simulations were performed in a Γ only point grid and with energy cutoff of 400 eV.

After the simulation, eight new optimization processes (for each concentration) were performed with fractional coordinates coming from each 5000 steps of the MD. The configurations with smaller energy for each concentration were captured as the ground state. Due to the great amount of calculations, in this part of the investigation, a cutoff of 400 eV and a Γ point mesh was set.

Once the ground state structure of each lithium concentration was found, then, new optimization were performed employing the hybrid functional method with a single Γ k-point mesh and a cutoff of 600 eV. Once the system have reached the required accuracy a new single point calculation were carried out with a k-point grid of 1x2x2 to derive the electronic and electrochemical properties. **The derived structures for the concentrations where $Nb_2O_2F_3$ would accept the insertion of Li atoms (0.25, 0.25, 0.75 and 1) are depicted in the Fig. 01 of the supplementary material.**

To finally ensure that niobium oxyfluoride can be applied as an anode material it is of utmost importance to have some insights of the lithium migration mechanism in its crystal structure. The climbing nudged elastic band method (cNEB) [25, 26] was employed to evaluate the activation energy of lithium ions hop from one equilibrium position to other. At this stage of the investigation a supercell of 2x2x2 containing 128 atoms was build up ensuring small interaction between periodic images. For the cNEB six replicas of the system were linearly interpolated between the two lithium equilibrium positions. The GGA approximation was applied with a cut of of 600 eV. The great dimension of the supercell allows a Brillouin zone sampling with a Γ only point centered k-mesh.

III. RESULTS

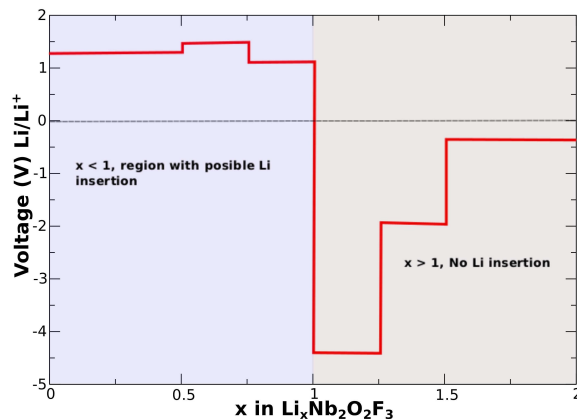$Nb_2O_2F_3$ was recently synthesized by Tran *et al.* [19] in a monoclinic I2/a space group with a phase transition

FIG. 1. Voltage profile diagram referent to the lithium deintercalation reaction for x varying from 0 to 2 in $Li_xNb_2O_2F_3$. From this picture it is possible to extract the maximum number of Li ions that can be inserted in the $Nb_2O_2F_3$ crystal structure per formula unit.

to a triclinic lattice, P1, at ~ 90 K. The $Nb_2O_2F_3$ crystal structure consist of NbX_6 (X=O or F) octahedra sharing edges of X and then forming Nb_2X_10 dimers. The dimers are linked by a sharing X atoms along c direction forming a kind of layered structure that allows the insertion of Li atoms. In fact, above 90 K, as reported by Tran *et al.*, Nb_2 dimers undergo a charge reordering from a +7 oxidation state to a system where half of the Nb_2 present +6 oxidation state and the other half reveal oxidation state of +8. These distinct charge ordering under 90 K and above 90 K is also the responsible for the symmetry break resulting in a phase transition from a monoclinic to a triclinic crystal structure.

Once a representative model for this material in all the Li ions concentration was derived, then the next step is to investigate the maximum capacity of lithium insertion under the battery reaction. In this scenario, the free energy of the transformation $Li_{x_0}Nb_2O_2F_3 + (x - x_0)Li^+ + (x - x_0)e^- \longrightarrow Li_xNb_2O_2F_3$ is computed by using Eq. 1 [28, 29]:

$$V = -\frac{E(Li_xNb_2O_2F_3) - (x - x_0)E_{Li} - E(Li_{x_0}Nb_2O_2F_3)}{(x - x_0)}$$

(1)

where E means the total energy of each related system and $x - x_0$ is the number of lithium ions participating in the reaction. For instance, in the transformation $Li_{0.25}Nb_2O_2F_3 \longrightarrow Li_{0.5}Nb_2O_2F_3$ x assumes the value of 0.5 and x_0 0.25 with $x - x_0$ reaching 0.25. The total energy of the metallic Li, E_{Li}, was calculated in the bcc structure, which is the structural phase of the Li anode. According to the definition of this equation the reaction will be most likely to occur until the potential is a positive value. Af-
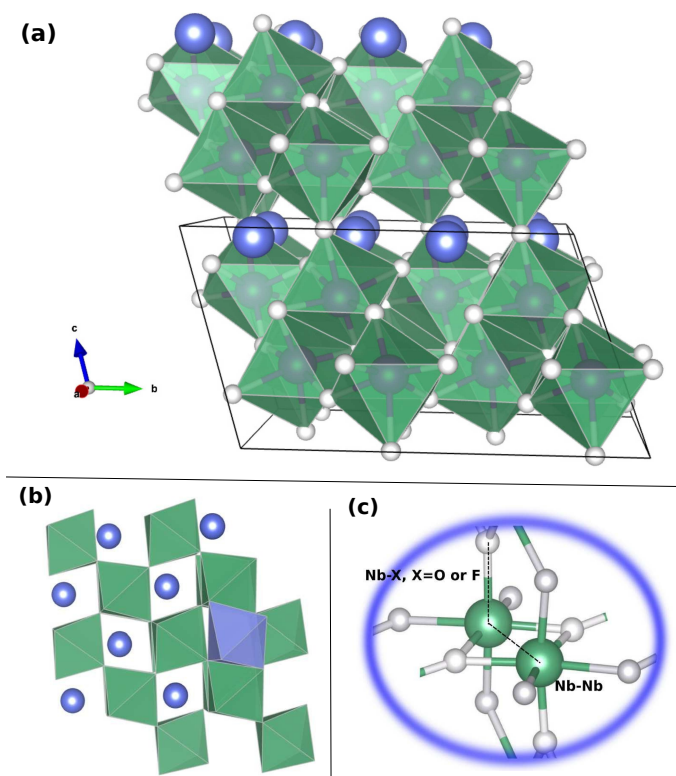
FIG. 2. (a)Crystal structure of $LiNb_2O_2F_3$. Here, the green color octahedra represents Nb_2X_{10} (X=O, F) dimers. White balls are O or F atoms. Blue balls are Li atoms. (b) Top view of the $LiNb_2O_2F_3$ crystal structure. The blue octahedra LiX_6 represents the position where the ions are placed. (c) Closer look on the Nb_2X_{10} dimer structure. There, it is possible to see the Nb-Nb bond and also the Nb-X bond. Information of the crystal structures of $Li_xNb_2O_2F_3$ is available in the supplementary material. This figure was produced using VESTA software [27]

ter that, it is expected in experiments that Li precipitate forming dendrites and disturbing the performance of the device.

Figure 1 is representing the voltage profile diagram used to evaluate the maximum lithium intercalation capacity. The transformation $LiNb_2O_2F_3 \longrightarrow Li_{1.25}Nb_2O_2F_3$ reveals a negative redox potential. Therefore, only one lithium per formula unit can be inserted in the niobium oxyfluoride crystal structure. Thus, considering $LiNb_2O_2F_3$ as the maximum stable capacity an average deintercalation potential of 1.29 V is evaluated. Of course, the revealed high average potential comes as a disadvantage for anode application since it diminishes the overall potential of cell. However, if the used cathode material presents a high voltage vs. Li/Li^+, then it is still worth to use $Nb_2O_2F_3$ as the anode with an average reduction of the potential of only 1.29 V.

Table I summarizes the evaluated lattice constants of the full lithiated and delithiated systems by using the

TABLE I. Computed lattice parameters and band gaps of $Nb_2O_2F_3$ for different Li concentration (x=0, 1) in the HSE06 method. The experimental values were extracted from Ref. [19][a].

Compound	a Å	b Å	c Å	α	β	γ	Å^3
$Nb_2O_2F_3$	5.18	5.72	6.971	108.92	111.68	90.03	179.58
Exp.[a] $Nb_2O_2F_3$	5.18	5.70	6.89	108.67	109.92	90.33	179.81
$LiNb_2O_2F_3$	5.28	5.78	7.09	108.29	112.05	90.00	189.10

framework of the hybrid functional and the reported experimental values of the delithiated structure. The revealed results are in reasonable good agreement with the reported experimental values for the niobium oxyfluoride lattice parameters. The main observed difference between the experimental triclinic $Nb_2O_2F_3$ and the relaxed structure derived here comes up with the bond distances analysis. After the optimization process all Nb_2 bond distances emerge with a value of 2.54 Å. Such a result is in disagreement with the reported values by Tran *et al.* [19] since the triclinic structure emerges with two non equivalent dimers where one has a shorter bond distance of 2.50 Å and the other presents a value of 2.65 Å. This difference is mainly due to a charge reordering leading to a mixed dimer valence state where half of the Nb_2 present +6 oxidation state and the other half show +8. This picture is not captured by the calculations where all Nb_2 bond distance display the same value such as for the reported monoclinic structure of oxyfluoride. Therefore, the main difference between both structural models is broken and a monoclinic like behavior is recovered here.

In this material lithium ions would likely to assume positions in between the Nb_2X_{10} layers as showed in Fig. 2. It is observed that the layers distance formed by Nb_2X_{10} units undergoes a change from 3.97 Å to 4.97 Åwith lithium insertion. This change results in a volume expansion of 5% in the framework of the $Nb_2O_2F_3$ crystal structure. Moreover, it is inferred that the local environment of the inserted Li ions shows X atoms forming octahedral units around Li positions as depicted by the blue octahedra in Fig. 2.

In order to have insights into the local structural and electronic changes under the intercalation of Li ions the bond length evolution of the pairs Nb-Nb and Nb-X are investigated. A shrinkage of the Nb-Nb bond length going from 2.54 Å to 2.39 Å is revealed over lithium insertion where the first and second values are referent to the delithiated and fulllithiated compound ($LiNb_2O_2F_3$). This smaller value of the Nb-Nb bond length comes due the reduction process experimented by the Nb_2 dimers going from +7 valence state to +6 valence state. This result is in agreement with the founds reported by Tran *et al.* [19] where dimers with +6 state present smaller Nb-Nb bond length than dimers with +7 valence state. The average bond length of the octahedra Nb-X in the lithiated materials present values around 2.12 Å. The difference between the Nb-X bond length for the host ma-
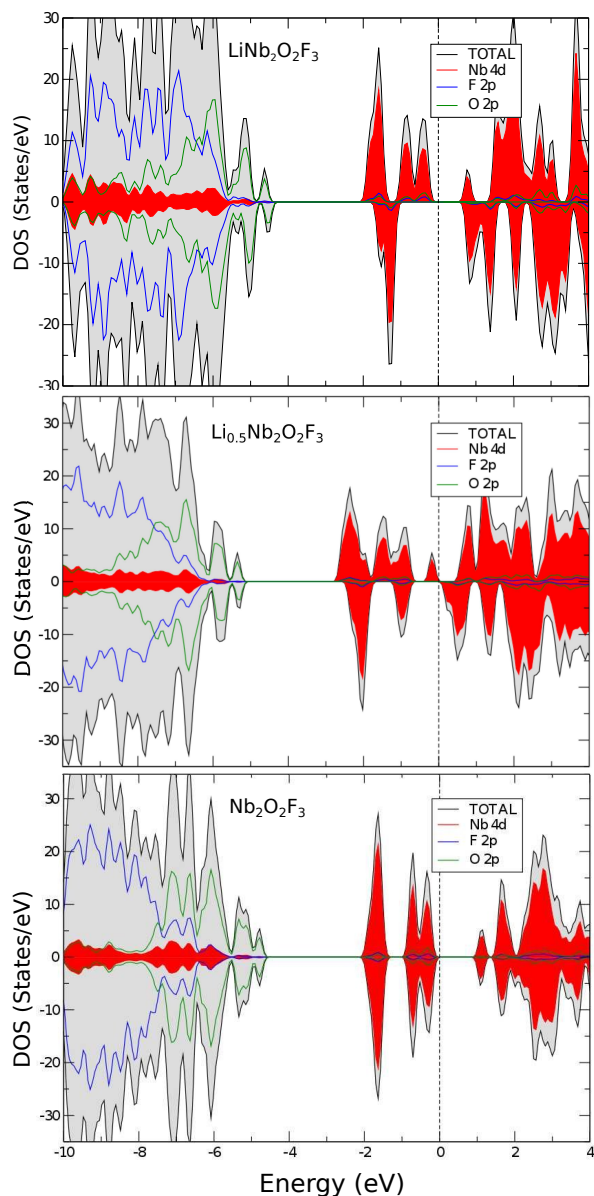
FIG. 3. Total and projected density of state (pDOS) evaluated for $LiNb_2O_2F_3$, $Li_{0.5}Nb_2O_2F_3$ and $Nb_2O_2F_3$. Gray color represents the total DOS, red color represents d states of Nb atoms summed up, blue lines represent p states of F atoms summed up and green lines represent p states of O atoms summed up.

terial 2.05 Å and the lithiated material is of the order of 0.06 Å. This small difference in the bond length indicates that extra electrons coming from Li atoms are not populating molecular orbitals formed by Nb-X states as it is usual for cathode materials [30]. From these results, it is possible to speculate that reduction reaction under Li insertion is occurring mainly in the Nb-Nb centers.

To further understand charge rearrangement over Li

insertion the Bader analysis method is employed [31, 32]. The average net charge computed here is defined as the charge computed with the Bader analysis minus the total charge of the referent specie. Nb atoms in the delithiated state are presenting an average net charge of +2.34. With the addition of Li atoms in the crystal structure of $Nb_2O_2F_3$ forming $LiNb_2O_2F_3$ this value goes to +2.02. It means that each pair Nb-Nb undergoes a reduction process receiving approximately one electron. The average net charge change of O and F atoms displays very small values amounting to +0.04 and +0.06 under lithiation. This result is in accordance with the structural analysis where Nb-Nb bond distances decrease with Li ions insertion whereas Nb-X bond length maintain almost the same value.

Figure 3 is showing the projected and total density of states (pDOS and DOS) of the $LiNb_2O_2F_3$, $Li_{0.5}Nb_2O_2F_3$ and $Nb_2O_2F_3$, respectively. The presented results are in completely accordance with the current trend of battery materials [33–35] where d states of transition metals dominate around the valence band maximum (VBM) and conduction band minimum (CBM). The revealed band gap of the host material $Nb_2O_2F_3$ is also in agreement with the reported by Tran *et al.* [19] reaching about 1 eV for the system where Nb_2 dimers have oxidation state +7. It is also worth to emphasize that the lithiation process in this system comes with a semiconductor to metal transition when half of Li atoms are inserted and, then, the semiconductor behavior is recovered when the other half lithium atoms are included as showed in Fig. 3.

By considering a molecular orbital picture of Nb-Nb bonds the t_{2g} coming from Nb-4d states would hybridize forming $\sigma^2 \pi^1$ filled molecular orbitals (MO) [19, 36, 37]. Then, the insertion of half Li atoms leads to a charge rearrangement where half of the Nb-Nb now have π^2 states while the other half Nb-Nb part is stil with π^1. The filling of the π^2 states is accompanied of a symmetry break of the system and then a transition from semiconductor to metal is observed as showed by the pDOS depicted in Fig. 3. In fact, the insertion of half Li atoms induce the semiconductor-metal transition and, then, the insertion of the other half lithium atoms emerge with a opened band gap again. In this scenario, by forming now $LiNb_2O_2F_3$ the symmetry of the crystal structure is recovered with all π molecular orbital filled with two electrons and a metal-semiconductor transition is observed. A very similar effect is reported by Ref. [19], where a phase transition is observed from the monoclinic to the triclinic crystal structure.

To have a better understand of the Li migration mechanisms in the crystal structure of $LiNb_2O_2F_3$ (full lithiated system) the cNEB method is employed to evaluate the activation energy of ions hop. Two main pathways were considered as the most likely and depicted in Fig. 4. Firstly, Li ions are allowed to hop through the layers of the structure (Pathway 01). Secondly, it is consid-
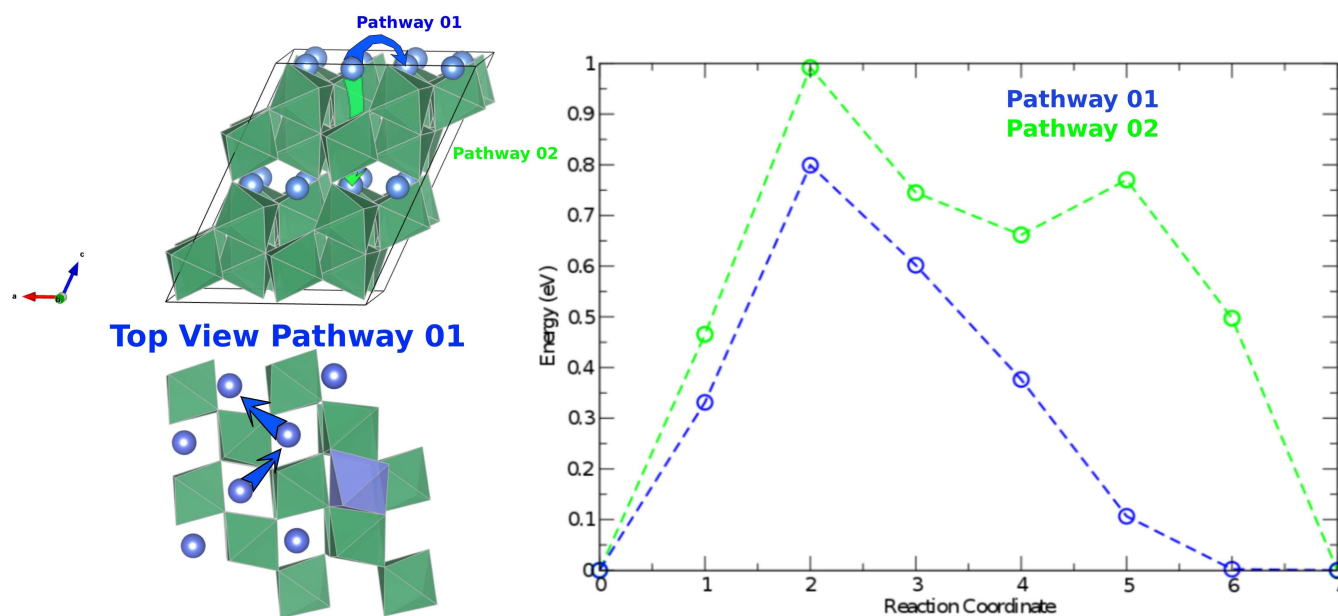
FIG. 4. Activation energy profile of the Li ions hop through Pathway 01, represented by blue color, and Pathway 02, represented by green color. It is also represented the top and side view of the $LiNb_2O_2F_3$ cristal structure with the investigated pathways.

ered the possibility of Li ions cross the Nb-X layers migrating through [0 0 1] direction (Pathway 02). The computed activation energies for the Li^+ hopping in these pathways amounts to 0.79 eV and 0.99 eV for Pathway 01 and 02, respectively. The higher value of the hop barrier revealed by Pathway 02 leads to a lower probability of Li ions diffusion occur in this direction. This is a result of the higher Coulombic repulsion felt by the Li^+ ion when crossing the Nb-X layers. Pathway 01 has presented activation energy of 0.79 eV being the most likely direction. This activation energy value induces Li ions to mostly migrate in the between of the formed layers resulting in a 2D like hopping mechanism.

producing small expansion of the crystal framework. A maximum of one Li atom per formula unit is inferred with an average potential of 1.29 V vs. Li/Li^+. The insertion of lithium atoms induce a semiconductor to metal transition with half of lithium in the host material. Then, when full lithiated, the semiconductor behavior is recovered with a small band gap of 1 eV. This small band gap together with a metal behavior during the insertion reaction indicates that $Nb_2O_2F_3$ can be used without the necessity of extra composites for the electronic conductance. Moreover, the ionic conductance should take place most likely in between the layers of the structure with hop activation energy of 0.79 eV for the Li ions migration. These results include niobium oxyfluoride for the first time to the map of possible materials for anode application.

IV.   CONCUSIONS

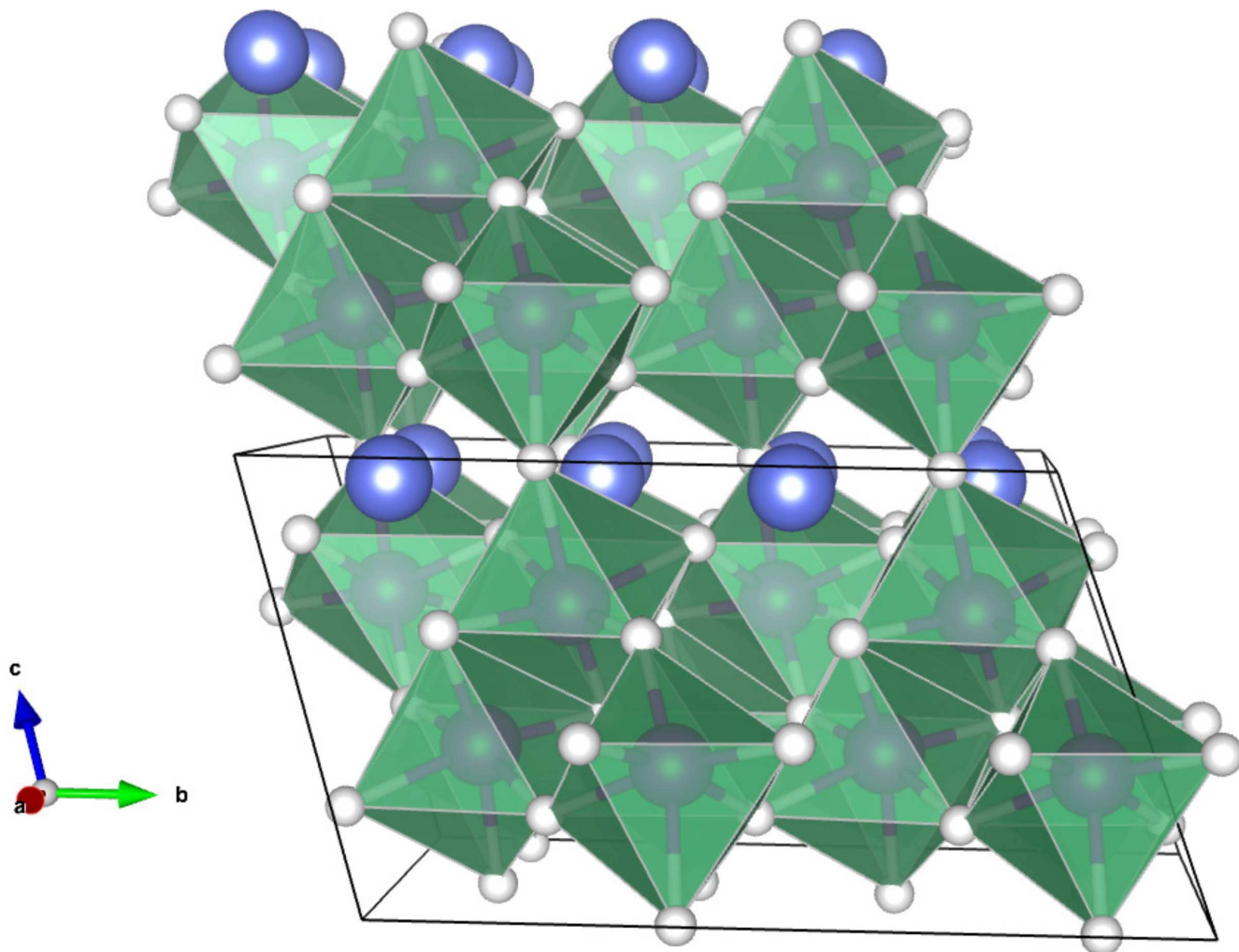In summary, the framework of the density functional theory was employed in order to investigate the electronic and structural evolution under lithium intercalation in $Nb_2O_2F_3$ for the first time. Lithium atoms display likely to place in between of the layers formed by Nb-F-O atoms

V.   ACKNOWLEDGEMENTS

[1] Q. Tang, Z. Zhou and P. Shen, *J. Am. Chem. Soc.* 2012, **134**, 16909

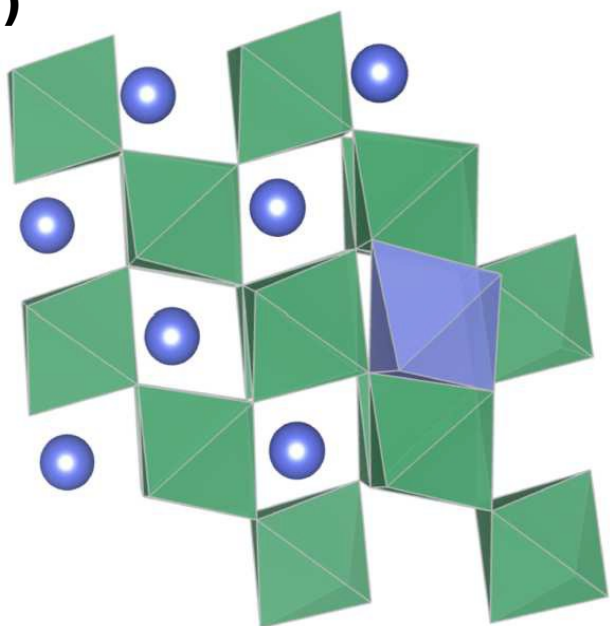[2] Y. Jing, Z. Zhou, C. R. Cabrera, and Z. Chen, *J. Phys. Chem. C*, 2013, **117**, 25409

[3] M. Catti and M. R. Ghaani, *Phys. Chem. Chem. Phys.*, 2014, **16**, 1385.

[4] S. H. Kang, D. P. Abraham, W. S. Yoon, K. W. Nam and X. Q. Yang, *Electrochim. Acta*, 2008, **54**, 684.

[5] M. A. Reddy and U. V. Varadaraju, *Chem. Mater.*, 2008, **20**, 4557.

[6] J. T. Han, D. Q. Liu, S. H. Song, Y. Kim and J. B. Goodenough, *Chem. Mater.*, 2009, **21**, 4753.

[7] J. T. Han and J. B. Goodenough, *Chem. Mater.*, 2011, **23**, 3404.

[8] N. Kumagai, Y. Koishikawa, S. Komaba and N. Koshiba, *J. Electrochem. Soc.*, 1999, **146**, 3203.

[9] R. Kodama, Y. Terada, I. Nakai, S. Komaba and N. Kumagai, *J. Electrochem. Soc.*, 2006, **153**, A583.

[10] Y. Li, D. Wu, Z. Zhou, C. R. Cabrera and Z. Chen, *J. Phys. Chem. Lett.* 2012, **3**, 2221.

[11] D. Wu, Z. Xie, Z. Zhou, P. Shen and Z. Chen, *J. Mater. Chem. A*, 2015, **3**, 19137.

[12] J. Bao , D. Wu , Q. Tang , Z. Ma and Z. Zhou, *Phys. Chem. Chem. Phys.*, 2014, **16**, 16145.

[13] R. A. Armstrong, G. Armstrong, J. Canales, R. Garcia, P. G. Bruce, *Adv. Mater.*, 2005, **17**, 862.

[14] K. Nakahara, R. Nakajima, T. Matsushima and H. Majima, *J. Power Sources*, 2003, **117**, 131.

[15] L. Cheng, H. J. Liu, J. J. Zhang, H. M. Xiong and Y. Y. Xia, *J. Electrochem. Soc.*, 2006, **153**, A1472.

[16] V. Pralong, M. A. Reddy, V. Caignaert, S. Malo, O. I. Lebedev, U. V. Varadaraju and B. Raveau, *Chem. Mater.*, 2011, **23**, 1915.

[17] R. J. Cava, D. W. Murphy and S. M. Zahurak, *J. Electrochem. Soc.*, 1983, **130**, 2345.

[18] J. Colin, V. Pralong, M. Hervieu, V. Caignaert and B. Raveau, *Chem. Mater.*, 2008, **20**, 1534.

[19] T. T. Tran, M. Gooch, B. Lorenz, A. P. Litvinchuk, M. G. SorollaII, J. Brgoch, P. C. W. Chu, and A. M. Guloy, *J. Am. Chem. Soc.*, 2015, **137**, 636.

[20] G. Kresse and J. Hafner, *Phys. Rev. B*, 1993, **47**, 558.

[21] G. Kresse and J. Hafner, *Phys. Rev. B*, 1996, **54**, 11169.

[22] J. P. Perdew, K. Burke and M. Ernzerhof, *Phys. Rev. Lett.*, 1996, **77**, 3865.

[23] J. Heyd, G. E. Scuseria and M. Ernzerhof, *J. Chem. Phys.*, 2003, **118**, 8207.

[24] J. Heyd, G. E. Scuseria and M. Ernzerhof, *J. Chem. Phys.*, 2006, **124**, 219906.

[25] H. Jonsson, G. Mills, and K. W. Jacobsen, in Classical and Quantum Dynamics in Condensed Phased Simulations, edited by B. J. Berne, G. Ciccotti, and D. F. Coker (World Scientific, River Edge, NJ, 1998), p. 385.

[26] G. Henkelman and H. Jonsson, *J. Chem. Phys.*, 2000, **113**, 9978.

[27] K. Momma and F. Izumi, *J. Appl. Crystallogr.*, 2011, **44**, 1272.

[28] M. K. Aydinol, A. F. Kohan, G. Ceder, K. Cho and J. Joannopoulos, *Phys. Rev. B*, 1997, **56**, 1354.

[29] R. P. Joshi, B. Ozdemir, V. Barone and J. E. Peralta, *J. Phys. Chem. Lett.*, 2015, **6**, 2728.

[30] A. Van der Ven, C. Marianetti, D. Morgan and G. Ceder, *Solid State Ionics*, 2000, **135**, 21.

[31] R. F. W. Bader, Atoms in Molecules: A Quantum Theory; Oxford University Press: New York, 1990.

[32] W. Tang, E. Sanville and G. Henkelman, *J. Phys.: Condens. Matter*, 2009, **21**, 084204.

[33] C. Frayret, A. Villesuzanne, N. Spaldin, E. Bousquet, J. Chotard, N. Recham and J. Tarascon, *Phys. Chem. Chem. Phys.*, 2010, **12**, 15512.

[34] S. C. Chung, P. Barpanda, S. I. Nishimura, Y. Yamada and A. Yamada, *Phys. Chem. Chem. Phys.*, 2012, **14**, 8678.

[35] F. Zhou, M. Cococcioni, C. A. Marianetti, D. Morgan and G. Ceder, *Phys. Rev. B*, 2004, **70**, 235121.

[36] R. J. Goddard, R. Hoffmann and E. D. Jemmis, *J. Am. Chem. Soc.* 1980, **102**, 7667.

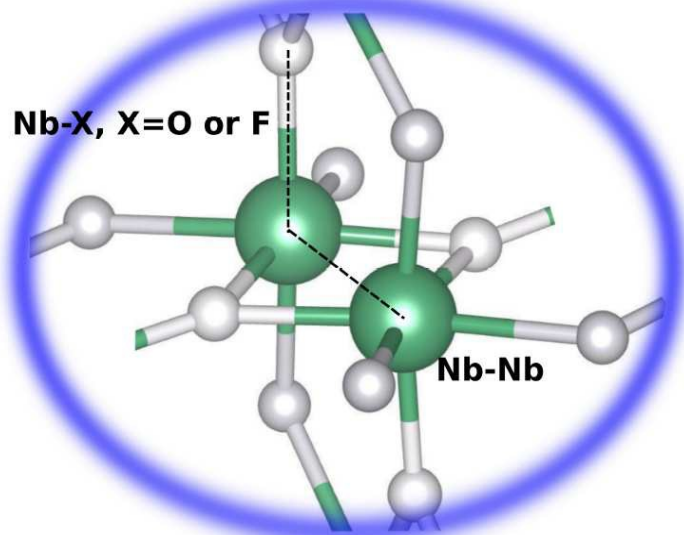[37] F. A. Cotton, M. P. Diebold, C. O'Connor and G. L. Powell, *J. Am. Chem. Soc.*, 1985, **10** , 7438.
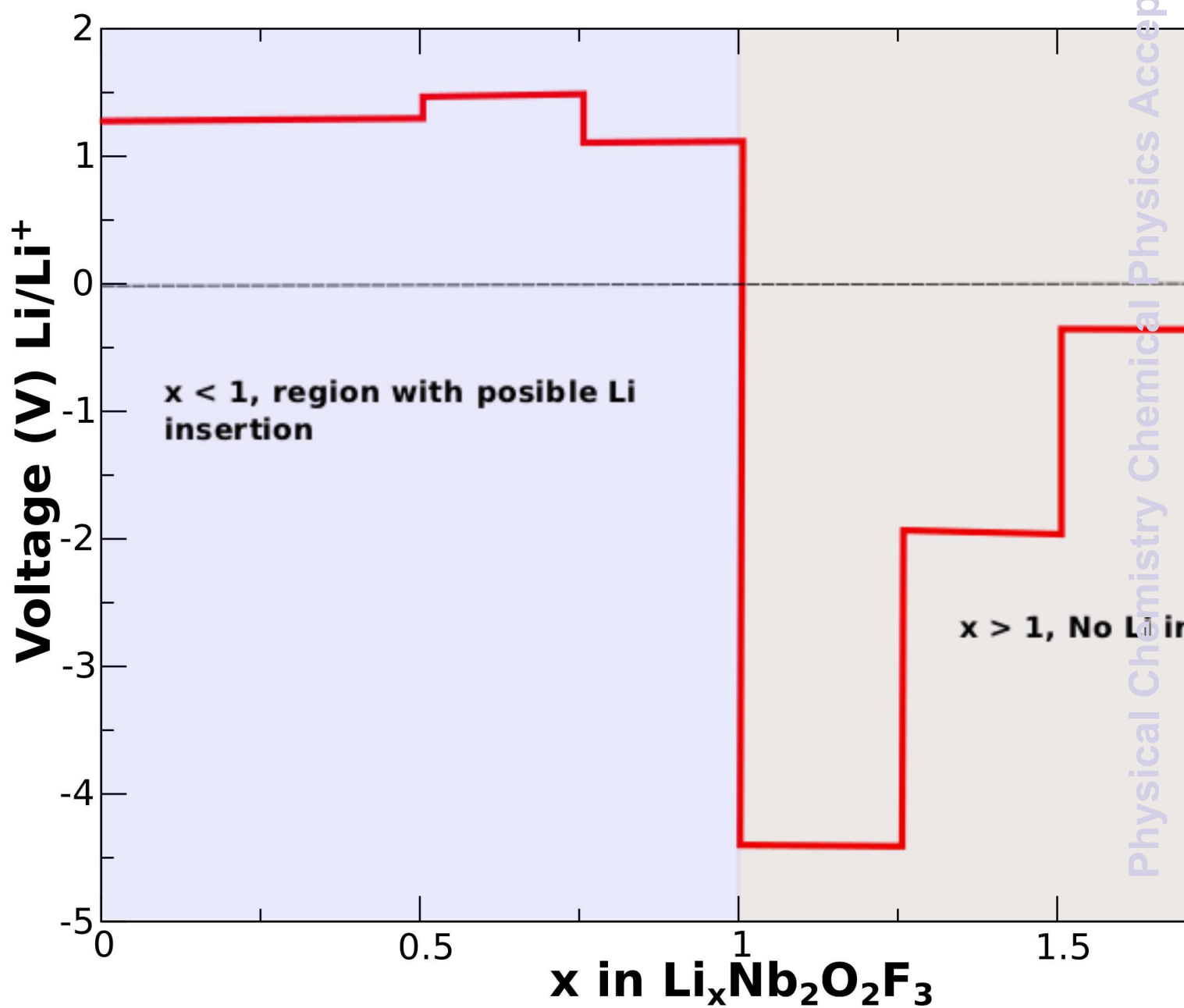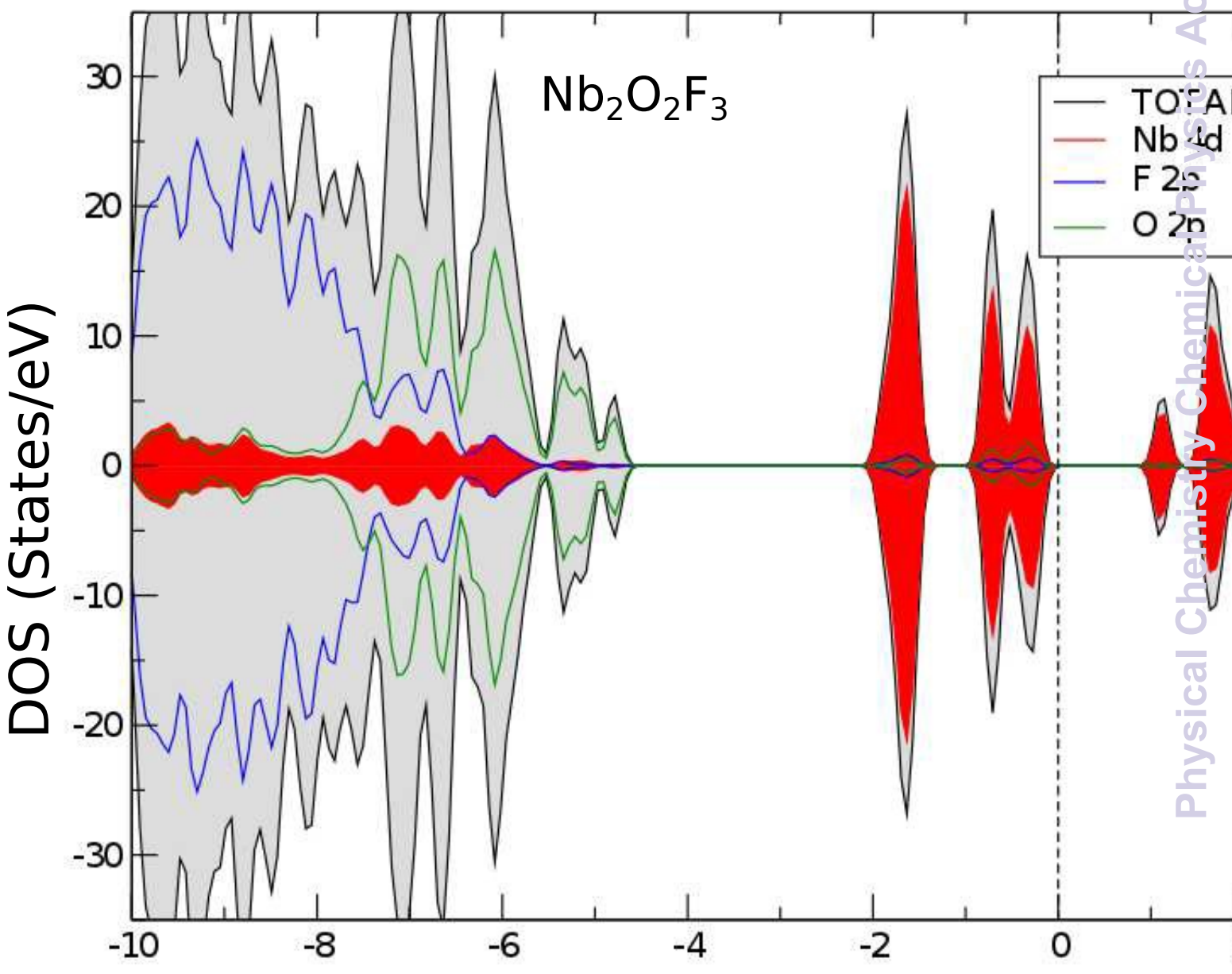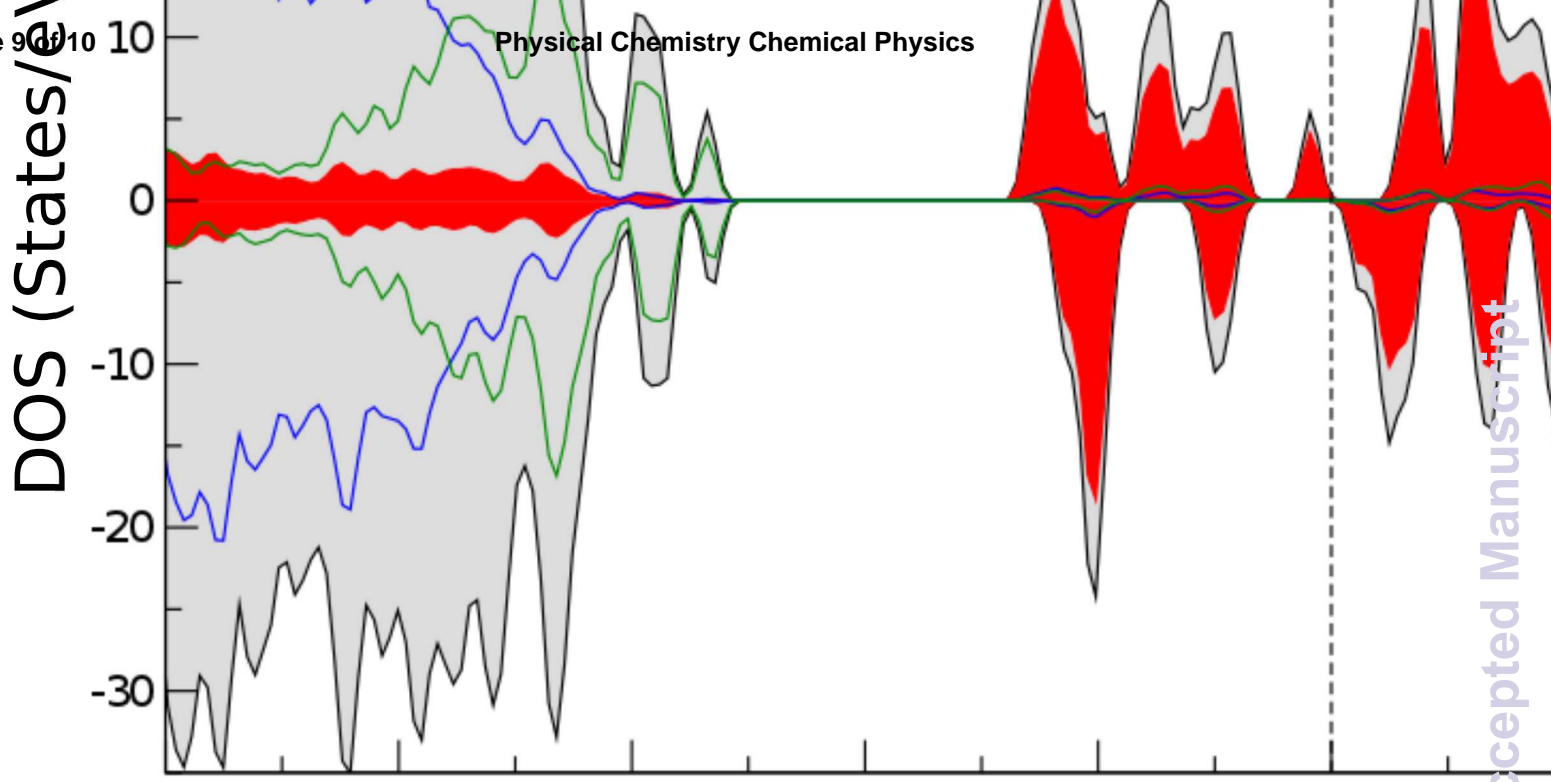
(a)

(b)

(c)

Nb-X, X=O or F

Nb-Nb

$Nb_2O_2F_3$

Legend:
- TOTAL
- Nb 4d
- F 2p
- O 2p

DOS (States/eV)

DOS (States/eV)

Energy (eV)

Pathway 01

Pathway 02

Top View Pathway 01